Semiconducting Electronic Structure of the Ferromagnetic Spinel $HgCr_2Se_4$ Revealed by Soft-X-Ray Angle-Resolved Photoemission Spectroscopy

Hiroaki Tanaka[1] Andrei V. Telegin,[2] Yurii P. Sukhorukov,[2] Vladimir A. Golyashov,[3,4] Oleg E. Tereshchenko,[3,4] Alexander N. Lavrov[5] Takuya Matsuda[1] Ryusuke Matsunaga[1] Ryosuke Akashi,[6] Mikk Lippmaa,[1] Yosuke Arai,[1] Shinichiro Ideta[7,*] Kiyohisa Tanaka,[7] Takeshi Kondo,[1,8] and Kenta Kuroda[9,10,†]

[1]*Institute for Solid State Physics, The University of Tokyo, Kashiwa, Chiba 277-8581, Japan*
[2]*M.N. Mikheev Institute of Metal Physics, UB RAS, Ekaterinburg 620108, Russia*
[3]*Institute of Semiconductor Physics, SB RAS, Novosibirsk 630090, Russia*
[4]*Synchrotron Radiation Facility SKIF, Boreskov Institute of Catalysis, SB RAS, Kol'tsovo 630559, Russia*
[5]*Nikolaev Institute of Inorganic Chemistry, SB RAS, Novosibirsk 630090, Russia*
[6]*Quantum Materials and Applications Research Center, National Institutes for Quantum Science and Technology, Meguro-ku, Tokyo 152-0033, Japan*
[7]*UVSOR Facility, Institute for Molecular Science, Okazaki, Aichi 444-8585, Japan*
[8]*Trans-scale Quantum Science Institute, The University of Tokyo, Bunkyo-ku, Tokyo 113-0033, Japan*
[9]*Graduate School of Advanced Science and Engineering, Hiroshima University, Higashi-hiroshima, Hiroshima 739-8526, Japan*
[10]*International Institute for Sustainability with Knotted Chiral Meta Matter (WPI-SKCM^2), Hiroshima University, Higashi-hiroshima, Hiroshima 739-8526, Japan*

We study the electronic structure of the ferromagnetic spinel $HgCr_2Se_4$ by soft-x-ray angle-resolved photoemission spectroscopy (SX-ARPES) and first-principles calculations. While a theoretical study has predicted that this material is a magnetic Weyl semimetal, SX-ARPES measurements give direct evidence for a semiconducting state in the ferromagnetic phase. Band calculations based on the density functional theory with hybrid functionals reproduce the experimentally determined band gap value, and the calculated band dispersion matches well with ARPES experiments. We conclude that the theoretical prediction of a Weyl semimetal state in $HgCr_2Se_4$ underestimates the band gap, and this material is a ferromagnetic semiconductor.

Angle-resolved photoemission spectroscopy (ARPES) is a powerful tool for investigating the electronic structure of solids because ARPES can directly observe band dispersions [1]. By comparing ARPES spectra with *ab initio* band calculations, it is possible to verify the presence of various emergent electronic properties, such as Weyl points in polar Weyl semimetals [2–5] and magnetic Weyl semimetals [6,7]. Density functional theory (DFT) [8,9] calculations are often used to predict the electronic structure of a material, but DFT calculations are known to underestimate the width of the band gap of solids [10]. The discrepancy between calculations and experiments can be eliminated with the help of hybrid functionals, where model parameters are adjusted to reproduce the experimentally determined materials' characteristics [11].

Among the materials showing very different characteristics in calculations and experiments, the ferromagnetic spinel $HgCr_2Se_4$ (space group $Fd\bar{3}m$, $T_C \simeq 110$ K) [12–16] is one of the most intriguing. Magnetotransport studies have reported that this material is an insulator [12] or either a *p*- or *n*-type semiconductor [17], depending on crystal growth conditions. Infrared optical measurements have observed a band gap of 0.3–0.8 eV depending on temperature [18–20]. The proposed *s-d* model [21] accounting for direct allowed transition at the Γ point and the band gap could explain the temperature dependence of electron mass and the anisotropy of the magnetoresistance of *p*-type materials [22]. On the other hand, recent DFT calculations using the generalized gradient approximation (GGA) for the exchange-correlation functional have predicted a semimetallic electronic structure and the presence of magnetic Weyl points near the Fermi level [23]. Their prediction and another study on pyrochlore iridates [24] are two of the earliest works of magnetic Weyl semimetals. Following the magnetic Weyl semimetal proposal, additional support for the Weyl semimetal state was found by the observation of the anomalous Hall effect (AHE) [25]. However, the AHE of $HgCr_2Se_4$ has an unconventional temperature dependence [26]. Since then, a theoretical study has suggested that the observed AHE temperature dependence may be extrinsic, caused by scattering, and unrelated to magnetic Weyl semimetals [27]. In addition, another report on the band dispersion of $HgCr_2Se_4$ [28] has claimed that the modified Becke-Johnson exchange-correlation functional [29] yields

a gapped magnetic semiconductor phase. To the best of our knowledge, the direct observation of the band dispersion by ARPES has been missing, and the real electronic structure of $HgCr_2Se_4$ is still under debate.

In this Letter, we report the first observation of the band dispersion of $HgCr_2Se_4$ by soft-x-ray (SX) ARPES. We observed only hole bands around the Fermi level and did not find any electron bands crossing them. This result unambiguously indicates that $HgCr_2Se_4$ has a semiconducting electronic structure in the ferromagnetic phase, which is consistent with the previously reported transport and optical properties [12,17–19]. Our accurate DFT calculations using hybrid functionals could reproduce the semiconducting band dispersion, and the calculated band dispersion agrees well with the experimental results. Our results highlight that a simple comparison of ARPES spectra with DFT calculations has to be handled with care.

Single crystals of $HgCr_2Se_4$ were grown by the chemical transport reaction technique using $CrCl_3$ as a carrier agent. The crystal structure was analyzed by powder x-ray diffraction (Supplemental Material Fig. S1 in Ref. [30]). We used three single crystals in the experiments; two of them (A and B) were p-type, and the other (C) was n-type. Since as-grown $HgCr_2Se_4$ crystals usually become p-type, the n-type crystals were obtained by annealing them in a Hg vapor [15,17,33–35]. A triangular face of a single crystal and the edge of the triangle [Fig. 1(a)] correspond to the (111) plane and the $[\bar{1}10]$ direction, respectively (Supplemental Material Note 2 in [30]). We set the xyz axes so that the x axis was parallel to the edge and the z axis was perpendicular to the plane [Figs. 1(a) and 1(b)]. The characteristics of $HgCr_2Se_4$ single crystals were examined by transport, magnetic, and infrared transmission analysis (Note 3 in the Supplemental Material [30]). SX-ARPES measurements were performed at BL25SU of SPring-8 [36], and supplemental ARPES measurements using vacuum ultraviolet (VUV) light were performed at BL5U of UVSOR. We used 400–550 eV SX light in SX-ARPES measurements and 60 eV VUV light in VUV-ARPES measurements. The measurement temperature was kept around 50 K. The samples were cleaved *in situ* in ultrahigh vacuum better than $\sim 3 \times 10^{-8}$ Pa. The cleaved surfaces were later examined by contact-mode atomic force microscopy (AFM) in air. The electronic band structures were calculated from first principles using the Quantum Espresso [37] and Wannier90 [38] packages (Note 3 in the Supplemental Material [30]). The charge density was calculated with the Kohn-Sham equation with the Heyd-Scuseria-Ernzerhof (HSE) 06 exchange-correlation functional [39,40]. After that, the Kohn-Sham bands were derived with the Wannier interpolation method [41,42]. The experimentally observed crystal structure was adopted, and spin-orbit coupling was included in the calculations.

We distinguished p- and n-types by the temperature dependence of the resistivity [Fig. 1(c)]; p-type crystals
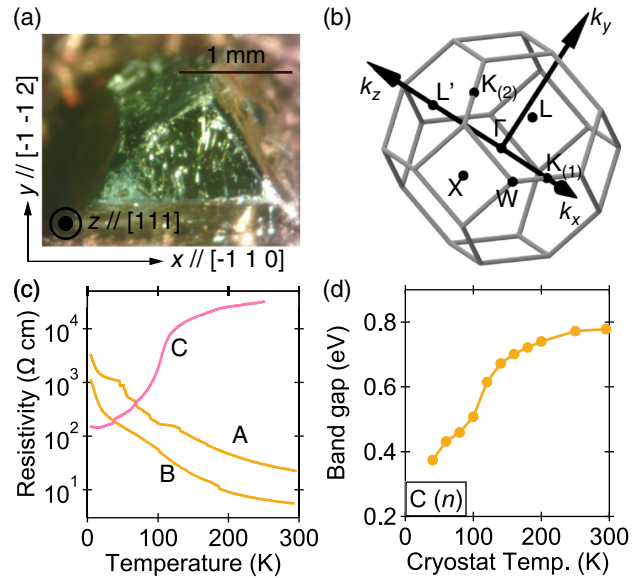

FIG. 1. Structure, transport properties, and optical properties. (a) Microscope image of an octahedral single crystal. (b) Brillouin zone and high-symmetric points. (c) Temperature dependence of the resistivity. (d) Temperature dependence of the band gap of crystal C (n-type) estimated from the transmittance spectra.

(A and B) exhibited increasing resistivity at lower temperature while the resistivity of an n-type crystal (C) dropped upon cooling at around $T_C \simeq 110$ K [17,25,33,43]. These conductivity types are consistent with the Seebeck coefficient signs determined by a hot-probe method at room temperature. We observed some steps and spikes in the $\rho - T$ curves. We think they can be due to the magnetic domain structure reformation with changing the temperature; the anomalous magnetoresistance behavior [Fig. S3(a) in the Supplemental Material [30]] indicates unconventional transport properties at the magnetic domain boundaries. Since the resistivity curve for the n-type sample is similar to that of metal, n-type $HgCr_2Se_4$ has been considered to be a degenerated semiconductor [17,33]. The magnetic property measurements showed ferromagnetic behavior below T_C [Figs. S3(b) and S3(c) in the Supplemental Material [30]]. The transmittance spectra of n-type $HgCr_2Se_4$ (crystal C) showed a steplike feature (Fig. S4 in the Supplemental Material [30]); the transmittance steeply dropped to nearly zero above a threshold, indicating the existence of a band gap. The band gap energy estimated from these spectra [Fig. 1(d)] exhibits a temperature dependence similar to previous studies [18–20]. Since the previous studies use p-type samples to measure the band gap, our measurements of the n-type sample clarify that the band gap behavior is independent of the carrier type. All these results are consistent with the previous reports claiming that $HgCr_2Se_4$ is a ferromagnetic semiconductor.

Using SX-ARPES, we present conclusive evidence for the semiconducting electronic structure of $HgCr_2Se_4$ in the
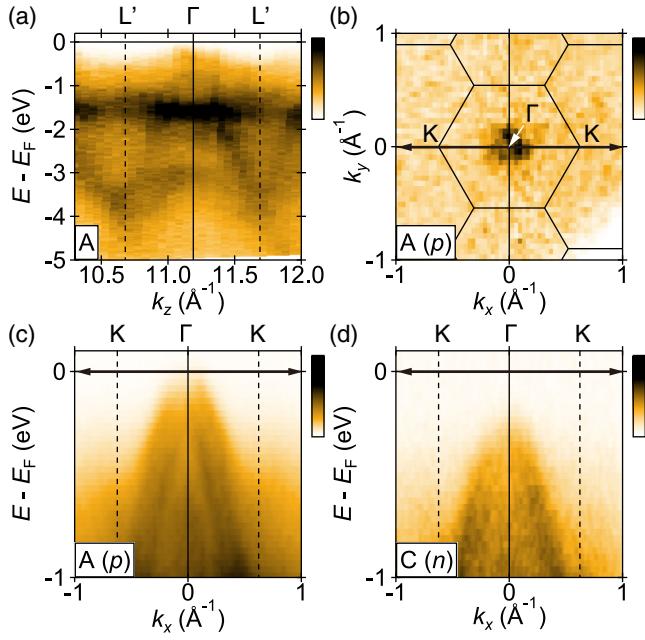
FIG. 2. SX-ARPES measurements. (a) k_z dispersion along the $\Gamma L'$ direction. (b) Fermi surface of crystal A (p-type). Black solid lines represent the cross section of the Brillouin zone. (c),(d) Band dispersions of crystals A (p-type) and C (n-type) along the ΓK direction [black arrow in (b)]. (b)–(d) were taken with 475 eV SX light.
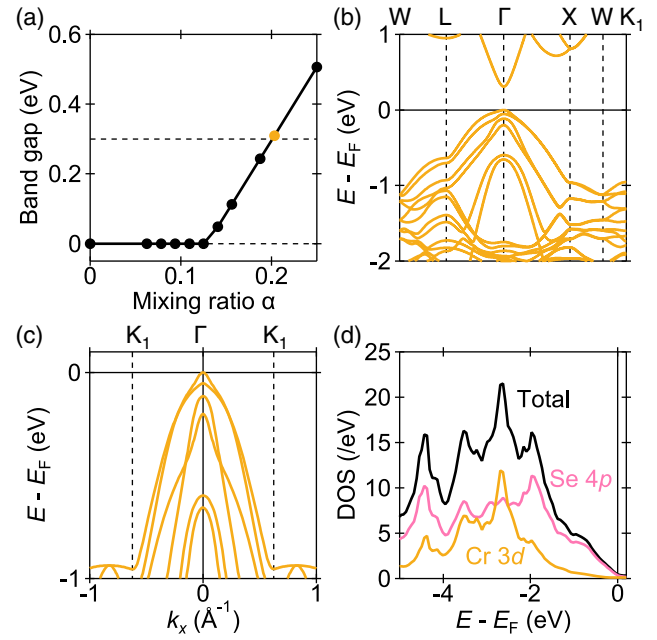

FIG. 3. DFT calculations. (a) Relation between the mixing ratio of Hartree-Fock exchange and the band gap. The horizontal dashed line at 0.3 eV represents the experimental band gap at low temperatures [19]. (b),(c) Band dispersions at the mixing ratio corresponding to the orange point in (a). (d) Density of states (DOS) of the valence bands.

ferromagnetic phase. We could observe band dispersions from all three samples. Figure 2(a) represents the k_z dispersion of HgCr$_2$Se$_4$ (crystal A) along the $\Gamma L'$ direction obtained by changing the photon energy from 400 eV to 550 eV. We used the inner potential of 12 eV and the work function of 5 eV to convert the photon energy to the wave vector. These values gave properly symmetric k_z dispersions about the Γ or L' points.

The k_z dispersion analysis revealed that the 475 eV SX light captures the bulk band dispersion around the Γ point. Figure 2(b) shows the Fermi surface of p-type HgCr$_2$Se$_4$, and Figs. 2(c) and 2(d) show the ΓK direction band dispersions of p- and n-type HgCr$_2$Se$_4$, respectively. All dispersions exhibit only hole bands around the Γ point. The top of the hole bands in the p-type sample [Fig. 2(c)] is close to the Fermi level, which is consistent with the p-type carrier of the sample. On the other hand, the hole bands in the n-type sample [Fig. 2(d)] are at a slightly lower energy than those of the p-type sample [Fig. 2(c)], reflecting the electron doping of the n-type sample. Note 6 in the Supplemental Material [30] discusses the energy level of the n-type sample obtained by the infrared absorption and ARPES measurements. While earlier band calculation [23] has predicted that the hole and electron bands would cross around the Γ point in the ferromagnetic phase, such electron bands were absent in the experimental results. Thus we conclude that HgCr$_2$Se$_4$ is a semiconductor in the ferromagnetic phase, not a magnetic Weyl semimetal in constrast to the theoretical prediction [23].

Although SX-ARPES measurements were successful, ARPES measurements using VUV light, which is typically used in studies of Weyl semimetals, could not detect any clear dispersion around the Fermi level (Note 6 in the Supplemental Material [30]). The difference in SX and VUV-ARPES results is caused by the rough cleaved surface of the spinel HgCr$_2$Se$_4$. We will argue this point later.

We further analyzed the electronic structure of HgCr$_2$Se$_4$ by DFT calculations with the HSE06 hybrid functional. In the HSE06 functional, α represents the mixing ratio of the Hartree-Fock exact exchange into the Perdew-Burke-Ernzerhof (PBE) exchange-correlation functional [44] of the GGA type; $\alpha = 0$ corresponds to the original PBE functional, and $\alpha = 0.25 \equiv \alpha_{HSE06}$ is the standard HSE06 value. The PBE functional gives a semimetallic band structure with magnetic Weyl points near the Fermi level [23]. However, the standard local density approximation and GGA exchange-correlation functionals often underestimate the band gaps of semiconductors, even occasionally yielding incorrect gap closing. That is why the exact exchange is included in hybrid functionals to mitigate this problem [11]. Recent first-principles examinations [45,46] have suggested that the optimum value of α for an accurate band gap prediction may be smaller in narrow-gap semiconductors. To see the robustness of the gap opening, we, therefore, calculated the electronic structure with various α between 0 and 0.25. Figure 3(a) shows the band gaps for

different α values. A nonzero mixing ratio α yields a gapped electronic structure for $\alpha > 0.12$ and the band gap increases with increasing α [Fig. 3(a)].

Here we show the calculated band structure with $\alpha = \alpha_{HSE06} \times 13/16$ [orange point in Fig. 3(a)], where the band gap (0.31 eV) was approximately the same as the experimental one at low temperatures [19]; as discussed above, the band gap size depends on the temperature but is independent of the carrier type. Note 7 in the Supplemental Material [30] represents the calculation result with $\alpha = \alpha_{HSE06}$. Figure 3(c) shows the band dispersion along the k_x direction, which agrees well with the experimental results [Figs. 2(c) and 2(d)]. While the magnetic moments of the calculated electronic structure are aligned along the vertical direction in Fig. 1(b), the symmetry lowering due to the ferromagnetism is negligible (Note 8 in the Supplemental Material [30]). The calculated density of states [Fig. 3(d)] shows the contribution of Cr $3d$ and Se $4p$ orbitals to the valence band, and the contribution of Cr $3d$ orbitals is consistent with our resonant PES measurements (Note 9 in the Supplemental Material [30]). Our DFT calculations exhibit that the hybrid functional with the appropriate mixing ratio reproduces both the band gap determined by infrared spectra and the band dispersion obtained by SX-ARPES.

As was noted earlier, the roughness of the cleaved surface of the spinel $HgCr_2Se_4$ affects photoemission spectra particularly in VUV-ARPES. The following argument about the rough surface illustrates the benefit of using SX-ARPES to observe the band dispersion of a material that does not have a good cleaving plane.

The AFM images in Figs. 4(a) and 4(b) compare the cleaved surfaces of $HgCr_2Se_4$ and Bi_2Se_3, which is a quintuple-layered material hosting topological surface states [47,48]. The cleaved surface of $HgCr_2Se_4$ is indeed rough, while Bi_2Se_3 exhibits large flat terraces with occasional steps, reflecting the layered structure. Compared to the flat surface assumed in typical ARPES measurements, the uneven surface of $HgCr_2Se_4$ will create an unusual situation when photoelectrons escape from the crystal to the vacuum. Although the electronic structure of the rough surface region can be greatly different from that of the bulk, the photoemission from such an incoherent electronic structure is expected to be very weak because, roughly speaking, the photoemission probability is determined by the matrix element of the ground state and the plane wave. Therefore we think our ARPES spectra come from the photoemission in the deeper region (Fig. S10 in the Supplemental Material [30]), in which the electronic structure is sufficiently related to the bulk. The clear k_z dispersion [Fig. 2(a)] and the coincidence with the calculated bulk band dispersion [Fig. 3(c)] support our argument.

In the three-step model [1], when a photoelectron escapes from the crystal, the out-of-plane component of the photoelectron wave vector is modified while the in-plane component is unchanged (Fig. S11 in the
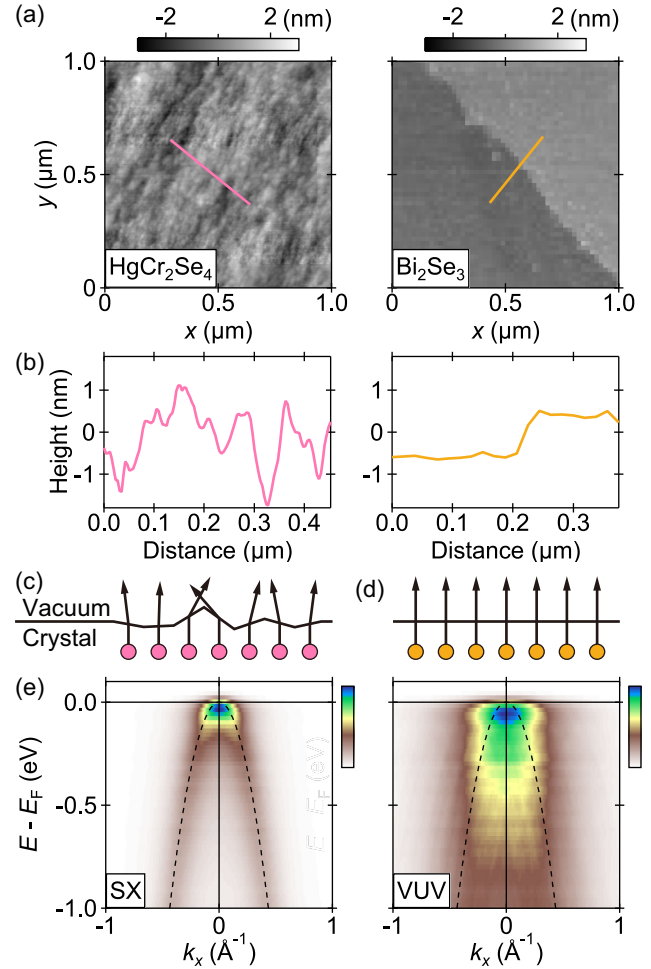

FIG. 4. Effect of surface roughness on ARPES spectra. (a) AFM images of $HgCr_2Se_4$ and Bi_2Se_3. Both panels use the same color scale. (b) Height profiles along the pink and orange lines in (a). (c),(d) Schematics of a rough surface modeled by randomly oriented flat surfaces and a flat surface. (e) Simulated photoemission spectra refracted by a rough surface in SX and VUV regions. The dashed parabolas represent the band dispersion before the refraction.

Supplemental Material [30]). While standard ARPES studies discuss the refraction of the photoelectron using a flat plane as shown in Fig. 4(d), such an analysis cannot be applied straightforwardly to $HgCr_2Se_4$ with a rough cleaved surface. We simulated the photoemission from a rough surface as a sum of photoemission spectra from randomly oriented flat surfaces [Fig. 4(c) and Ref. [49]] using the hole band dispersion in Fig. 2(c). The simulated spectra in the SX and VUV regions are shown in Fig. 4(e) for photon energies that are approximately the same as in the experiments. A slightly broadened parabolic dispersion is retained in the SX region. However, the simulated spectra in the VUV region are too broad to see a dispersion curve. The constant energy maps also exhibit similar behavior (Fig. S12 in the Supplemental Material [30]). This difference arises because the wave vector of a photoelectron in

the VUV region is shorter than that in the SX region and, therefore, more strongly refracted (Fig. S13 in the Supplemental Material [30]). A clear advantage of SX-ARPES over VUV-ARPES is thus that SX-ARPES can be used to study materials that are not easy to cleave and therefore suffer from increased surface roughness. We note that the bulk sensitivity of SX-ARPES [50] and a microfocused beam of a dedicated SX-ARPES beamline [36] can also contribute to the clear dispersion observed in the SX-ARPES experiments.

In conclusion, we show for the first time the ARPES result of the ferromagnetic spinel $HgCr_2Se_4$, which is direct evidence for the semiconducting electronic structure of this material. SX-ARPES was used to visualize the valence band dispersion of $HgCr_2Se_4$. We only observed hole bands while electron bands were absent below the Fermi level. These ARPES results are consistent with the existence of a band gap determined by infrared transmittance spectra. DFT calculations with the HSE06 hybrid functional reproduced the gapped band dispersion. We adjusted the mixing ratio of the HSE06 functional so that the calculations gave the experimentally observed band gap, and obtained dispersion curves that agreed well with our ARPES result. Our study draws attention to choosing appropriate functionals in DFT calculations and the advantage of SX-ARPES in investigating the electronic structure of solid crystals.

[*]Present address: Hiroshima Synchrotron Radiation Center, Hiroshima University, Higashi-hiroshima, Hiroshima 739-0046, Japan.

[†]kuroken224@hiroshima-u.ac.jp

[1] J. A. Sobota, Y. He, and Z.-X. Shen, Rev. Mod. Phys. 93, 025006 (2021).

[2] S.-Y. Xu et al., Science 349, 613 (2015).

[3] B. Q. Lv, N. Xu, H. M. Weng, J. Z. Ma, P. Richard, X. C. Huang, L. X. Zhao, G. F. Chen, C. E. Matt, F. Bisti, V. N. Strocov, J. Mesot, Z. Fang, X. Dai, T. Qian, M. Shi, and H. Ding, Nat. Phys. 11, 724 (2015).

[4] L. X. Yang, Z. K. Liu, Y. Sun, H. Peng, H. F. Yang, T. Zhang, B. Zhou, Y. Zhang, Y. F. Guo, M. Rahn, D. Prabhakaran, Z. Hussain, S.-K. Mo, C. Felser, B. Yan, and Y. L. Chen, Nat. Phys. 11, 728 (2015).

[5] M.-Y. Yao, N. Xu, Q. S. Wu, G. Autès, N. Kumar, V. N. Strocov, N. C. Plumb, M. Radovic, O. V. Yazyev, C. Felser, J. Mesot, and M. Shi, Phys. Rev. Lett. 122, 176402 (2019).

[6] K. Kuroda et al., Nat. Mater. 16, 1090 (2017).

[7] D. F. Liu, A. J. Liang, E. K. Liu, Q. N. Xu, Y. W. Li, C. Chen, D. Pei, W. J. Shi, S. K. Mo, P. Dudin, T. Kim, C. Cacho, G. Li, Y. Sun, L. X. Yang, Z. K. Liu, S. S. P. Parkin, C. Felser, and Y. L. Chen, Science 365, 1282 (2019).

[8] P. Hohenberg and W. Kohn, Phys. Rev. 136, B864 (1964).

[9] W. Kohn and L. J. Sham, Phys. Rev. 140, A1133 (1965).

[10] W. G. Aulbur, L. Jönsson, and J. W. Wilkins, Quasiparticle Calculations in Solids, edited by H. Ehrenreich and F. Spaepen, Solid State Physics Vol. 54 (Academic Press, New York, 2000), pp. 1–218.

[11] M. Marsman, J. Paier, A. Stroppa, and G. Kresse, J. Phys. Condens. Matter 20, 064201 (2008).

[12] P. K. Baltzer, H. W. Lehmann, and M. Robbins, Phys. Rev. Lett. 15, 493 (1965).

[13] P. K. Baltzer, P. J. Wojtowicz, M. Robbins, and E. Lopatin, Phys. Rev. 151, 367 (1966).

[14] K. Minematsu, K. Miyatani, and T. Takahashi, J. Phys. Soc. Jpn. 31, 123 (1971).

[15] A. Selmi, M. Heritier, and P. Gibart, Prog. Cryst. Growth Charact. 13, 121 (1986).

[16] N. Bebenin, R. Zainullina, and Y. P. Sukhorukov, J. Magn. Magn. Mater. 387, 127 (2015).

[17] L. Goldstein, P. Gibart, and A. Selmi, J. Appl. Phys. 49, 1474 (1978).

[18] H. Lehmann and F. Emmenegger, Solid State Commun. 7, 965 (1969).

[19] T. Arai, M. Wakaki, S. Onari, K. Kudo, T. Satoh, and T. Tsushima, J. Phys. Soc. Jpn. 34, 68 (1973).

[20] M. Auslender, E. V. Barsukova, N. Bebenin, B. Gizhevskii, N. Loshkareva, Y. P. Sukhorukov, and N. Chebotaev, Sov. Phys. JETP **68**, 139 (1989).

[21] M. Auslender and N. Bebenin, Solid State Commun. **69**, 761 (1989).

[22] V. A. Kostylev, B. A. Gizhevskii, A. A. Samokhvalov, M. I. Auslender, and N. G. Bebenin, Phys. Status Solidi (b) **158**, 307 (1990).

[23] G. Xu, H. Weng, Z. Wang, X. Dai, and Z. Fang, Phys. Rev. Lett. **107**, 186806 (2011).

[24] X. Wan, A. M. Turner, A. Vishwanath, and S. Y. Savrasov, Phys. Rev. B **83**, 205101 (2011).

[25] T. Guan, C. Lin, C. Yang, Y. Shi, C. Ren, Y. Li, H. Weng, X. Dai, Z. Fang, S. Yan, and P. Xiong, Phys. Rev. Lett. **115**, 087002 (2015).

[26] S. Yang, Z. Li, C. Lin, C. Yi, Y. Shi, D. Culcer, and Y. Li, Phys. Rev. Lett. **123**, 096601 (2019).

[27] S. Li and A. Levchenko, Phys. Rev. Lett. **124**, 156802 (2020).

[28] S.-D. Guo and B.-G. Liu, J. Phys. Condens. Matter **24**, 045502 (2012).

[29] F. Tran and P. Blaha, Phys. Rev. Lett. **102**, 226401 (2009).

[30] See Supplemental Material at http://link.aps.org/supplemental/10.1103/PhysRevLett.130.186402 for additional experimental and simulation data, which includes Refs. [31,32].

[31] M. van Setten, M. Giantomassi, E. Bousquet, M. Verstraete, D. Hamann, X. Gonze, and G.-M. Rignanese, Comput. Phys. Commun. **226**, 39 (2018).

[32] M. Maeda, K. Yamamoto, T. Mizokawa, N. L. Saini, M. Arita, H. Namatame, M. Taniguchi, G. Tan, L. D. Zhao, and M. G. Kanatzidis, Phys. Rev. B **97**, 121110(R) (2018).

[33] A. Selmi, P. Gibart, and L. Goldstein, J. Magn. Magn. Mater. **15–18**, 1285 (1980).

[34] N. I. Solin and S. V. Naumov, J. Exp. Theor. Phys. Lett. **72**, 612 (2000).

[35] N. I. Solin, V. V. Ustinov, and S. V. Naumov, Phys. Solid State **50**, 901 (2008).

[36] T. Muro, Y. Senba, H. Ohashi, T. Ohkochi, T. Matsushita, T. Kinoshita, and S. Shin, J. Synchrotron Radiat. **28**, 1631 (2021).

[37] P. Giannozzi et al., J. Phys. Condens. Matter **29**, 465901 (2017).

[38] G. Pizzi et al., J. Phys. Condens. Matter **32**, 165902 (2020).

[39] J. Heyd, G. E. Scuseria, and M. Ernzerhof, J. Chem. Phys. **118**, 8207 (2003).

[40] J. Heyd, G. E. Scuseria, and M. Ernzerhof, J. Chem. Phys. **124**, 219906 (2006).

[41] N. Marzari and D. Vanderbilt, Phys. Rev. B **56**, 12847 (1997).

[42] I. Souza, N. Marzari, and D. Vanderbilt, Phys. Rev. B **65**, 035109 (2001).

[43] J. P. Sun, Y. Y. Jiao, C. J. Yi, S. E. Dissanayake, M. Matsuda, Y. Uwatoko, Y. G. Shi, Y. Q. Li, Z. Fang, and J.-G. Cheng, Phys. Rev. Lett. **123**, 047201 (2019).

[44] J. P. Perdew, M. Ernzerhof, and K. Burke, J. Chem. Phys. **105**, 9982 (1996).

[45] A. Alkauskas, P. Broqvist, and A. Pasquarello, Phys. Status Solidi (b) **248**, 775 (2011).

[46] J. H. Skone, M. Govoni, and G. Galli, Phys. Rev. B **89**, 195112 (2014).

[47] H. Zhang, C.-X. Liu, X.-L. Qi, X. Dai, Z. Fang, and S.-C. Zhang, Nat. Phys. **5**, 438 (2009).

[48] Y. Xia, D. Qian, D. Hsieh, L. Wray, A. Pal, H. Lin, A. Bansil, D. Grauer, Y. S. Hor, R. J. Cava, and M. Z. Hasan, Nat. Phys. **5**, 398 (2009).

[49] The source code and the input files for the simulation are available from https://github.com/Hiroaki-Tanaka-0606/Photoelectron_refraction.

[50] V. Strocov, L. Lev, M. Kobayashi, C. Cancellieri, M.-A. Husanu, A. Chikina, N. Schröter, X. Wang, J. Krieger, and Z. Salman, J. Electron Spectrosc. Relat. Phenom. **236**, 1 (2019).

[51] Y. Ishida and S. Shin, Rev. Sci. Instrum. **89**, 043903 (2018).

Correction: A proof request to remove the third affiliation and its indicator for the second and third authors in the original front matter was incorrectly fulfilled and has been set right.